Proceedings of the 39th IAHR World Congress
19-24 June 2022
Granada, Spain
DOI number

Interaction of Short Wind Waves and Swell: An Experimental and Numerical study.

Antoine Villefer[1,2], Michel Benoit[1,2], Damien Violeau[1,2], Maria João Teles[1], Christopher Luneau[3] and Hubert Branger[4]

[1] EDF R&D Laboratoire National d'Hydraulique et Environnement (LNHE), Chatou, France
antoine.villefer@edf.fr; michel.benoit@edf.fr; maria.teles@edf.fr

[2] Laboratory for Hydraulics Saint-Venant, Chatou, France
damien.violeau@edf.fr

[3] Institut Pythéas, Aix Marseille Univ, CNRS, IRD, Marseille, France
christopher.luneau@osupytheas.fr

[4] Aix Marseille Univ, CNRS, Centrale Marseille, Institut de Recherche sur les Phénomènes Hors-Equilibre (UMR 7342), Marseille, France
branger@irphe.univ-mrs.fr

Abstract

The accurate modelling and prediction of bimodal sea states, combining swell and wind waves, is of upmost importance for many applications such as wave overtopping of coastal protections. Yet, the discrepancy in the field observations and the wave model limitations make the modeling of this common sea state condition rather complex. The question guiding this paper is: are wind waves generated the same way with and without pre-existing swell? The approach we chose starts with laboratory measurements in a wind-wave facility showing that wind-sea growth is modified in the presence of long waves (representing swell). To upscale this observation to open oceans, a numerical spectral wave model is firstly validated by comparison with laboratory results, and then at coastal scale using *in situ* bimodal sea-state observations collected during the SHOWEX campaign. By a separation of the physical processes involved in wind-wave generation, numerical simulations allow to assess the role each physical process plays in the wind-wave growth when a swell system is present.

Keywords: complex sea states; wind-wave growth; wind-wave tank; wave model; wave spectra

1. INTRODUCTION

Although complex sea states composed of at least two different wave systems (i.e. swell and local wind-sea) occur rather frequently in the ocean, their dynamics is not entirely understood. However, it is crucial to model their properties (i.e. significant wave height, representative period, main direction, etc.) with precision for many industrial applications like wave overtopping and flood forecasting in coastal areas. In order to better assess the effect of swell on the generation of local wind-sea and to study the interaction between the two wave systems, physical experiments combined with numerical simulations using a third-generation wave model have been carried out.

Using the IRPHE/Pythéas wind-wave tank facility in Marseilles (France), wind-wave growth is observed with and without the presence of following irregular paddle waves (generated from a JONSWAP-type spectrum) representing the swell system. But, contrary to what has been observed in the past with a monochromatic swell (Donelan 1987), the irregular paddle-waves do not have a marked damping effect on the wind-wave energy. Thus, irregular paddle-waves significantly modify wind-wave development at laboratory scale in terms of wind-wave steepness due to a frequency downshift. However, only little evidence of interactions between both wave systems is observed at prototype scale (Hwang *et al.* 2011).

Since ideal wind-over-swell conditions are difficult to measure accurately in the ocean, numerical simulation is used as a bridge from laboratory to prototype scale. Thus, the validation of the model has been carried out at both scales. Initially designed for applications from global to coastal scales, the capabilities of a third-generation wave model in reproducing bimodal sea states at laboratory scale are investigated. Using the wave model TOMAWAC (Benoit *et al*. 1996) (part of the TELEMAC-MASCARET hydro-informatic system), an original set of source/sink terms of the action balance equation, describing wind input, white-capping dissipation and nonlinear four-wave interactions, is compared to the obtained experimental results in one hand, and to *in situ* measurements from the SHOWEX campaign (Zhang *et al.* 2009, Ardhuin *et al*. 2007) on the other hand.

Our methodology is presented by starting with the description of the laboratory experiments carried out in Marseilles wind-wave tank and the observation of the modified wind-wave growth in section 2. In section 3, a particular event of the SHOWEX campaign providing a valuable database to validate a wave model of wind-wave growth in the presence of swell is briefly described. Both laboratory and SHOWEX data are then used to validate TOMAWAC wave model introduced in section 4. The validation step, described in section 5, provides first insights about the processes at play in the wind-wave growth modification in the presence of swell.

2. THE LABORATORY EXPERIMENTS

2.1 The facility

The Institut de Recherche sur les Phénomènes Hors-Equilibre (IRPHE)–Pythéas wind-wave tank consists of a closed-loop tunnel with a 1.5 m high air cavity for air circulation above a basin with a 40 m long and 2.60 m wide test section (Figure 1). Waves can be generated either by the circulating air flow, by using an air blower, or by a mechanical wavemaker situated at the upwind end of the water tank. A more detailed description of the facility and the experiments is given in Villefer *et al*. (2021).

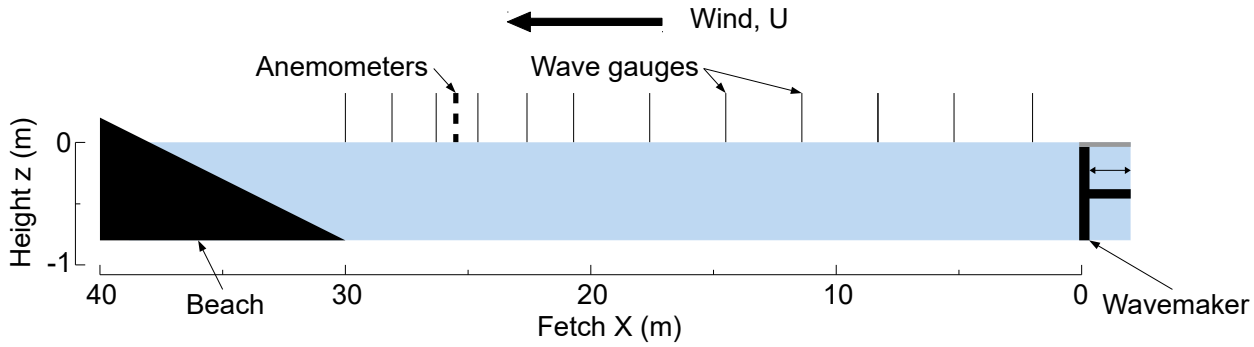

Figure 1. Sketch of the IRPHE/Pythéas wind-wave tank facility showing the location of the measuring devices. The vertical exaggeration is ×5.

2.2 The experiments

Both ways of generating waves were used to create a bimodal sea state within the test section: wind waves using the air-blower and long waves, representing swell, using the wavemaker. A set of 12 wave gauges measured free surface elevation time-series from which wave variance density spectra $E(f)$ were computed, with f the frequency, from a fetch of 2 m (gravity-capillarity wind waves) to 30 m (full gravity wind waves).

Both the effects of monochromatic and irregular long-crested swell on wind waves were studied. In this paper however, only cases with irregular swell are considered. The irregular swell was characterized by a JONSWAP-type spectrum with a peak frequency f_p = 0.6 Hz and two different values of steepness ak of 2.7 and 4.2 %, with $a = \sqrt{2m_0} = H_{m_0}/(2\sqrt{2})$ the representative wave amplitude, $m_0 = \int E(f)df$ the total variance of the free surface elevation and k the peak wave-number.

For wind-wave generation, the wind velocity could vary between 2 and 14 m.s^{-1}. Three wind velocity settings, measured with a sonic anemometer, were chosen for our study: U_{ref} = 6, 10 and 14 m.s^{-1}. The wind velocity profile $U(z)$ (i.e. vertical profile of the horizontal velocity) was measured using a hot film anemometer supported by a vertical telescopic pole. Fitting the measured velocities with a logarithmic profile, using Monin and Obukhov's (1954) turbulence similarity theory, permitted to obtain the friction velocity at the air/sea interface $u_\star$ and the aerodynamic roughness z_0.

2.3 The results

The analysis carried out in this section focusses on the comparison between the different spectra in terms of wave energy and peak frequency.

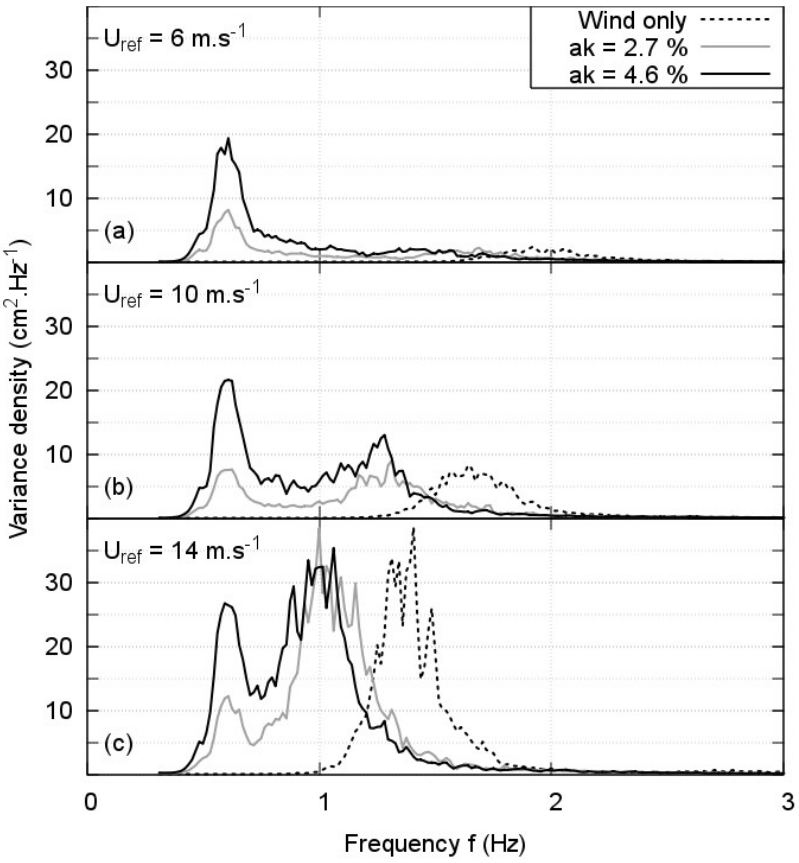

Figure 2. Measured wind-wave variance density spectra with and without irregular paddle waves of steepness ak and peak frequency 0.6 Hz for three wind velocities U_{ref} at fetch 30 m (maximal fetch).

In Figure 2, the comparison between the peaks of the dotted line spectra (obtained with wind waves only) and the corresponding high frequency peaks of both grey and black solid line spectra (obtained with wind-wave + irregular paddle waves) depicts a clear downshift of the wind-wave peak in the presence of long mechanically-generated waves. This downshift seems to increase with increasing swell steepness. Except for Figure 2.b. where the steepest long waves increase wind-wave energy, all the cases show a comparable level of energy of the wind-sea peak, independently of the presence and steepness of the long waves. Based on this observation, it is not clear that the long-wave system modifies the wind-wave energy.

Based on Villefer *et al*. (2021) observations, the friction velocity at the air/sea interface, which was considered as constant along the tank, tended to increase in the presence of long waves. This remark can be retained as a first hypothesis to explain the downshift of the wind-wave frequency. All these observations resulting from the laboratory experiments are expected to be encountered with the numerical simulations in the following.

3. SHOWEX OBSERVATIONS

The Shoaling Waves Experiment (SHOWEX) was conducted in the North Carolina continental shelf (east coast of the USA) from August to December 1999 (Ardhuin *et al*. 2003a,b). A cross-shelf transect of six Datawell Directional Waverider buoys, situated between 5 and 80 km (X1 to X6) from the coastline (see Figure 3), completed by three Air–Sea Interaction Spar (ASIS) buoys, were deployed to measure wave and wind properties. Extra data regarding the wind field in the area were provided by the stations of the National Data Buoy Center (NDBC) and the U.S. Army Corps of Engineers (USACE).

The event selected for TOMAWAC's validation happened on 3rd November 1999. This same event was chosen by Ardhuin *et al*. (2007) to validate the spectral wave model WAVEWATCH III (WW3) with *in situ* idealized fetch-limited conditions. A 10 m.s^{-1} wind, coming from the land (west wind, orange arrow in Figure 3), was blowing steadily and uniformly over a time period of 5 hours from 12:00 to 17:00 EST (East-Coast Standard Time). The direction of the wind was 10 to 30 degrees relative to the normal to the coast (i.e. slightly oblique wind). A moderate southeasterly swell (blue arrow in Figure 3) with a peak period $T_p \sim 10$ s and a significant wave height $H_s \sim 1$ m was nearly opposed to the local wind. Using measurements from several stations, the given air temperature was 6 to 10° colder than the ocean: the atmospheric boundary layer was thus unstable.

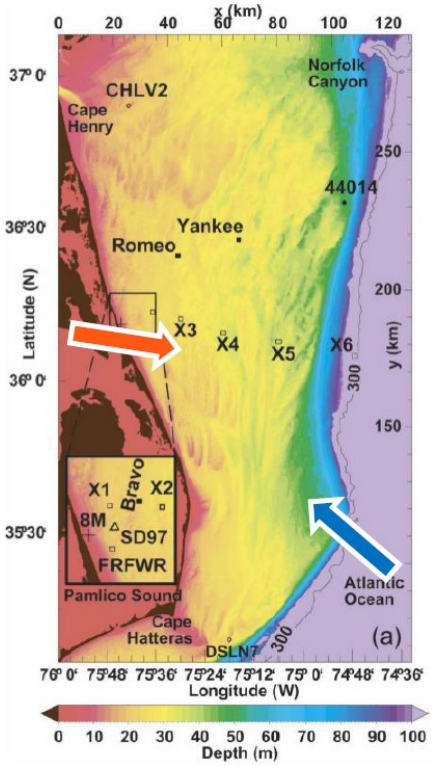

Figure 3. Bathymetry of the North Carolina shelf and locations of wave measurements during SHOWEX (1999). The orange and the blue arrows depict wind and swell directions respectively. (Figure reprinted from Ardhuin *et al*. 2007)

During this event, the observed wave spectra depicted the evolution of two well-defined wave systems: the high-frequency part with wind waves growing with fetch from X1 to X6 and the low frequency part with swell decreasing from offshore to the coast.

The idealized fetch-limited condition and the comparison with WW3 performances in reproducing the observations (Ardhuin *et al*. 2007, Ardhuin *et al*. 2010) provide a valuable database for TOMAWAC's validation.

4. WAVE MODEL

4.1 Brief presentation of TOMAWAC

TOMAWAC is a third-generation wave model (developed by the EDF R&D LNHE) using the finite element formalism for solving the balance equation of the action density directional spectrum in the sea domain (Benoit *et al*. 1996). To serve that purpose, the model computes the evolution of the action spectrum at each node of a spatial computational grid. In TOMAWAC the directional wave spectrum is split into a finite number of propagation frequencies f_i and directions θ_j. The balance equation of wave action density is solved for each component (f_i, θ_j). Each component of the action density spectrum changes in time under the combined effects of the several physical processes, modelled in the code.

The balance equation of the action density directional spectrum $N(t, \boldsymbol{x}, f, \theta)$ can be written as follow:

$$\frac{\partial N}{\partial t} + \dot{\boldsymbol{x}}\frac{\partial N}{\partial \boldsymbol{x}} + \dot{f}\frac{\partial N}{\partial f} + \dot{\theta}\frac{\partial N}{\partial \theta} = Q(t, \boldsymbol{x}, f, \theta) \quad [1]$$

The left part of the equation is the kinematic part and the right part gathers the contributions from the physical processes modeled using source/sink terms $Q(t, \boldsymbol{x}, f, \theta)$. In deep water, Q is usually formulated as:

$$Q = Q_{in} + Q_{ds} + Q_{nl} \quad [2]$$

corresponding to the processes of wind energy input Q_{in}, dissipation through white-capping Q_{ds} and nonlinear four-wave interactions Q_{nl}. In the following, water-current interaction is not considered, being the relative and absolute frequencies equal. Thereby, the variance density $E(f)$ is used instead of the action density ($E = 2\pi f N$).

Several parameterizations are available to compute each source term in TOMAWAC. In order to simulate the combination of swell and wind waves, the parametrization of the source terms needs to be carefully selected.

4.2 Parameterization of source terms

The standard TOMAWAC parameterization uses the WAM cycle 4 which was the default parameterization used in the operational forecasting at the European Centre for Medium-Range Weather Forecasts (ECMWF). This parameterization uses the Discrete Approximation Method (DIA), developed by Hasselmann *et al*. (1985), to account for the nonlinear four-wave interactions Q_{nl}. The transfer of momentum from the wind to the sea (Q_{in}) is given by Janssen's (1991) formulation. Lastly, the energy loss through white-capping (Q_{ds}) is estimated by Komen *et al*.'s (1984) sink term based on Hasselmann's (1974) work in which whitecaps act as a pressure pulse draining the energy from the wave.

Regarding the parameterizations chosen for TOMAWAC validation in the following, the WAM cycle 4 set of source terms is adapted by replacing the dissipation model of Komen *et al*. (1984) by a more recent one, partly based on a saturation threshold, developed by van der Westhuysen (2007) and based on Alves and Banner's (2003) work.

The use of this saturation-based model is motivated by the limitation of the pressure pulse model that uses an averaged wave steepness to estimate the dissipation. When using this latter model, the addition of mild swell leads to an anomalous amplification of a pre-existing wind-wave system: the low steepness of the swell reduces the mean dissipation rate.

Van der Westuysen (2007) developed a dissipation model taking the advantage of both the saturation-based model Q_{ds}^{W} and the pressure pulse one Q_{ds}^{K}, and proposed the following expression:

$$Q_{ds} = f_{br}(k).\, Q_{ds}^{W} + \left(1 - f_{br}(k)\right).\, Q_{ds}^{K} \qquad [3]$$

with

$$f_{br}(k) = \frac{1}{2} + \frac{1}{2}\tanh\left\{10\left[\left(\frac{B(k)}{B_r}\right)^{\frac{1}{2}} - 1\right]\right\} \qquad [4]$$

The ratio of the direction integrated saturation spectrum $B(k)$ over the saturation threshold B_r handles the weighting between both components of the dissipation term. That way, the energy of steep waves exceeding the saturation threshold is dissipated according to Q_{ds}^{W}, independently from the average steepness of the sea state, while the energy of milder waves is dissipated according to Q_{ds}^{K}. Hence, this formulation is relatively well adapted to bimodal sea-states modelling with the dissipation of steep wind waves becoming independent from the swell system.

The performances of this combination of source terms to reproduce the laboratory experiment first, and the November 3rd, 1999 SHOWEX event secondly, are showed and discussed in the next section.

5. VALIDATION

5.1 At laboratory scale

First, it is important to note that the validation of a 3rd generation wave model using direct laboratory measurements (i.e. without any kinematic similarity) is not common in the literature. This can be explained by the fact that such wave models are exclusively parameterized for wave hindcasting or forecasting at global, regional or coastal scales. However, as Shemer (2019) showed, wave generation in wind-wave tunnels is, to a great extent, comparable to *in situ* wind-wave growth. Thus, taking the advantage of the well-controlled laboratory environment, it can be a powerful way to validate 3rd generation wave models.

A first series of simulations lead to some adjustments of the parameterization of source terms. First, the wave growth limiter is deactivated. This limiter is generally used to guarantee the numerical stability of the calculation which, in our case, appears to be unnecessary with a small time step of 0.1 s. Secondly, in Janssen's (1991) wind-wave generation model (Q_{in}), the friction velocity at the air/sea interface is forced to be constant and equal to the laboratory measured one, without swell and for each wind speed. Without this forcing, the model tends to overestimate the friction velocity. Lastly, the approximation of infinite depth is adopted in the model since it was shown by Villefer *et al*. (2021) that the dissipation due to bottom friction is relatively low.

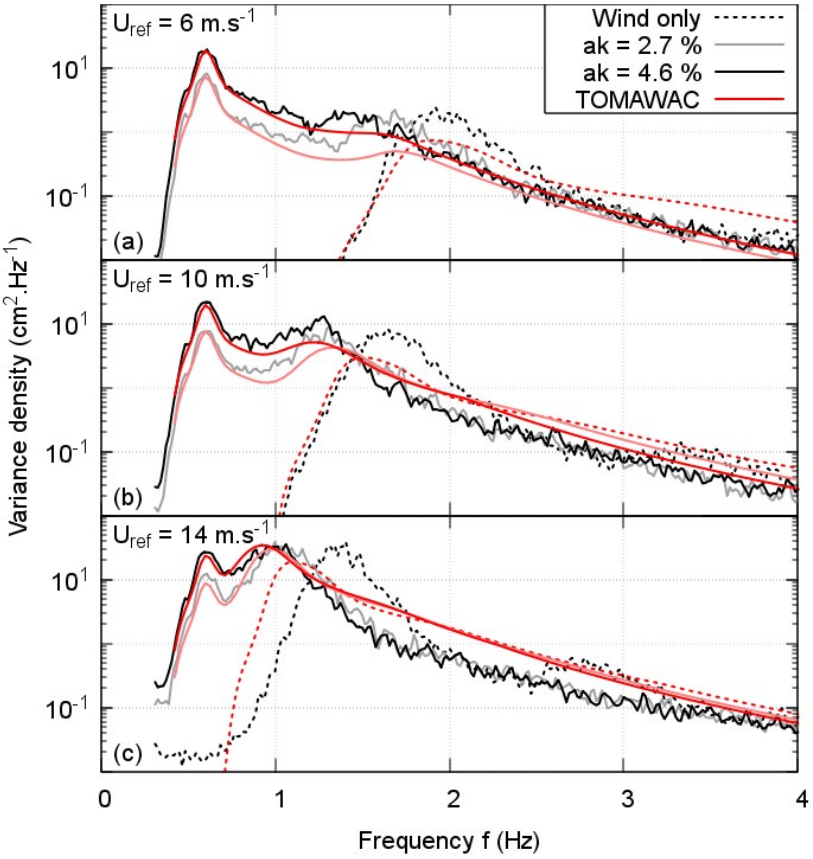

Figure 4. Measured (gray scale) and simulated (red scale) wind-wave variance density spectra with and without irregular paddle waves of steepness ak and peak frequency 0.6 Hz for three wind velocities U_{ref} at fetch 30 m (maximal fetch).

Figure 4 compares the variance spectra obtained with TOMAWAC at a 30-m-fetch with the experimental spectra. Overall, a good agreement between gray-scale and red-scale spectra is observed with the bimodal spectra (solid lines). Looking at each spectrum from the lowest to the highest frequencies, the swell peak, situated at 0.6 Hz, is well represented by the simulation at low wind speed (Figure 4.a) but slightly over dissipated when the wind speed increases (Figure 4.c) especially with swell of steepness $ak = 2.7$ %. At higher frequency and when swell is present, the simulated wind-wave peak agrees with the measurements in terms of peak frequency, but the corresponding energy levels are underestimated at low wind-speed. Without swell, the simulated wind-wave peak agrees with the shape of the low frequency side of the measured peak for Figure 4.a and 4.b. but fails to reproduce both the energy levels and the peak frequencies observed in the measurements. Lastly, the simulated high frequency tails of the spectra (above 2 Hz) look rather accurate when U_{ref} is equal to 6 and 10 m/s both in terms of energy level and slope but differ in terms of energy slope with the strongest forcing wind U_{ref} = 14 m.s^{-1}.

The slight increase of the swell dissipation in Figure 4.c can find an explanation considering the dissipation model of Komen *et al*. (1984). This model is activated in van der Westhuysen (2007) model for the swell's low frequency range (see eq. [3-4]). Hence, the high steepness of the wind waves penalizes the swell dissipation. This issue shows the limitation of van der Westhuysen (2007) model to simulate the low frequency waves for bimodal spectra when steep wind waves are present. A dissipation model free from the influence of the average wave steepness of the sea state, such as developed by Ardhuin *et al*. (2010), could help resolving this issue.

An interesting feature to observe in the TOMAWAC's simulations in Figure 4 is that, though the wind-wave peak frequency and energy are underestimated without swell, one can observe a slight deviation of the wind-wave peak towards the low frequency when the swell system is added. Thus, the wind-wave peak frequency

downshift observed in laboratory also happens in the simulations, to a lesser extent though. Since the friction velocity is kept the same with and without swell, this observation shows that the increase of the friction velocity is not sufficient to explain the downshift as it was assumed in section 2. A further analysis could permit to identify which source/sink term is involved in this modification of the wind-wave system.

Removing the friction velocity forcing, adopted for the simulations at laboratory scale, would be necessary to further improve TOMAWAC. Recent studies proposed a more accurate calculation of the friction velocity with the use of a wave boundary layer model by Du *et al*. (2017), or with Janssen and Bidlot's (2021) revision of Janssen's (1991) source term by further including the effects of nonlinearity.

Overall, TOMAWAC seems rather adapted to simulate the wind-wave growth in presence of a swell, as measured in the wind-wave tank. After this validation step at a laboratory scale and in order to upscale the observations, the wave-model performances must be verified at coastal scale with bimodal sea-state conditions.

5.2 At coastal scale

With several wave gauges distributed at different distances from the coast, the SHOWEX campaign is particularly adapted to the validation of a wave model. The bathymetry of Duck coastal shelf was included in TOMAWAC's calculation to take the variable water depth into account (Figure 5). It was also necessary to include a realistic wind field with variations in time and space. For that purpose, the model was forced with winds from Climate Forecast System Reanalysis (CFSR) files produced by the National Center for Environmental Prediction (NCEP). The swell coming from the south-east was estimated from buoy X6 data and imposed in the calculation at the south and east boundaries conditions of the numerical domain (illustrated in Figure 5).

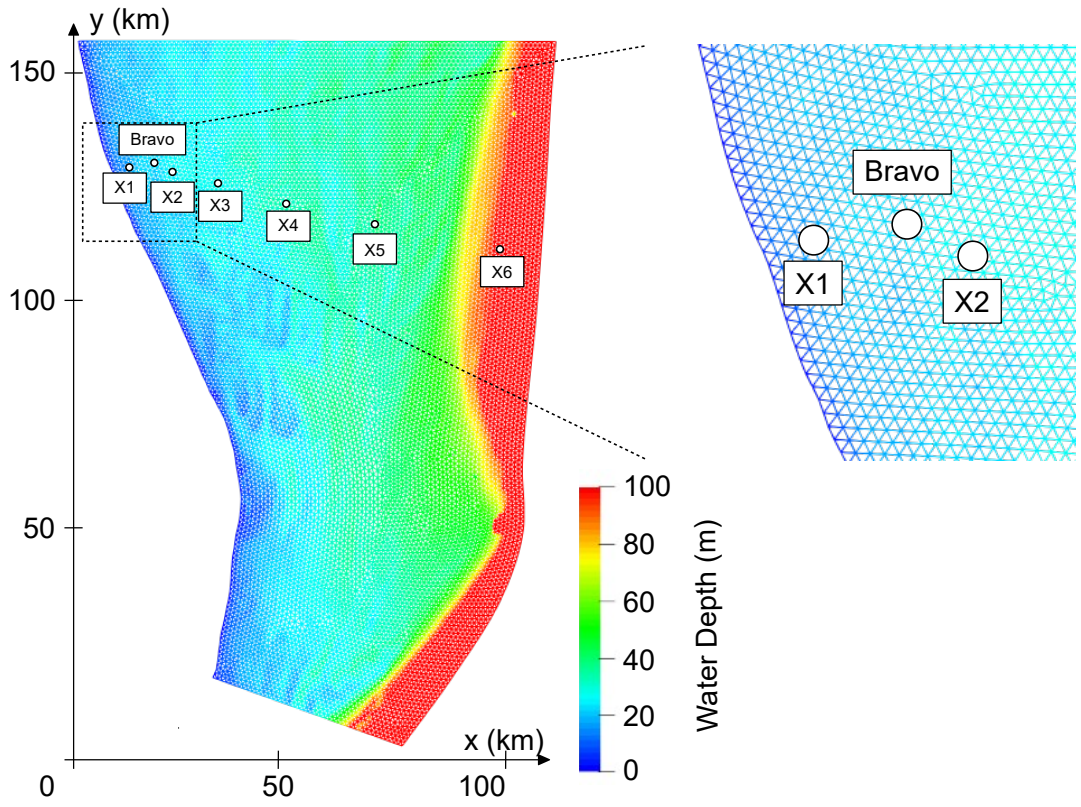

Figure 5. TOMAWAC's spatial domain showing the water depth and the irregular mesh adopted for the simulations. The distance between two consecutive nodes is 1 km.

The model was run from 2 November 23:00 EST to 3 November 17:00 EST. The first 13 hours of the run aimed at initializing the simulation starting from rest. The wave spectra used for comparisons with observations were averaged over the 12:00-17:00 EST time frame.

Figure 6 shows TOMAWAC's performances in reproducing the fetch-limited event by comparison with SHOWEX observations and simulations with WW3 using the ST4 parameterization of source/sink terms, proposed by Ardhuin *et al*. (2010), especially regarding the dissipation model. The gray zone highlights the wind-wave frequency range for each buoy.

TOMAWAC's frequency spectra (Figure 6.a and 6.d) are in rather good agreement with the observations. Regarding the mean directions, the simulation is quite accurate in the wind-wave frequency range. Especially, it is interesting to observe the wind-wave alongshore component reproduced in the simulation in Figure 6.b. However, the wind-wave directional spreading is underestimated by more than 10° for both buoys X1 and X3. Finally, TOMAWAC's results are close to be equivalent to the ones from ST4 parameterization by Ardhuin *et al*. (2010) based on the observations at buoy X3. Considering SHOWEX observations at buoy X3, the major improvement using ST4 would be the accurate capture of the energy spectrum around the local minimum between swell and wind-sea peaks (Figure 6.d) and the better agreement with the observed directional spread (Figure 6.f).

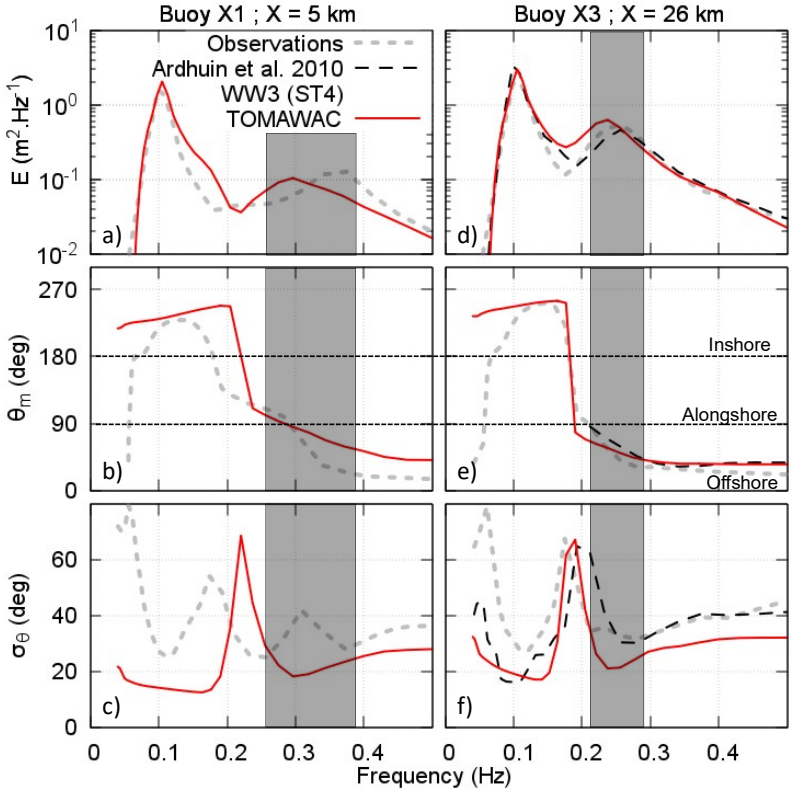

Figure 6. Simulated (solid red and dashed black lines) and observed (dotted gray line) (a,d) frequency spectra, and both as a function of frequency, (b,e) mean directions and (c,f) directional spreading on 3 Nov. 1999 (averages over the 12:00–17:00 EST time interval) at two fetches: 5 km and 26 km. Parameterization WW3 ST4 is the one proposed by Ardhuin *et al*. (2010).

6. CONCLUSIONS

Overall, the 3rd generation spectral model TOMAWAC performs well in reproducing wind-wave growth in the presence of swell, both at laboratory scale and at coastal scale. The parameterization using van der Westhuysen's (2007) dissipation source term, Janssen's (1991) wind input term and DIA parameterization to account for the nonlinear 4-wave interactions seems well adapted for simulating bimodal sea states. Based on the comparisons at buoy X3, ST4 parameterization (Ardhuin *et al*. 2010) gives somewhat equivalent results as TOMAWAC with the chosen parameterization but seems to better capture both the separation between the wave systems and the directional spreading. Given these first conclusions, TOMAWAC could be used for numerically assessing wind-wave growth in the presence of swell under various conditions (limited depth, strong/mild swell, etc.).

The followed methodology indicates that a wave model can be used as a bridge from laboratory to prototype scale. In this case, the controlled condition of a wind-wave tank revealed the downshift of the wind-wave frequency due to the presence of a preexisting following swell. Considering the validation at laboratory and coastal scales, the numerical model could be used as a tool to assess the extent at which the physical phenomena observed in laboratory can occur in open seas.

7. ACKNOWLEDGEMENTS

Antoine Villefer acknowledges the financial support of his PhD research program provided by the French ANRT (Association Nationale de la Recherche et de la Technologie) with CIFRE Grant 2019-1257. The authors thank Fabrice Ardhuin (LOPS, UMR 6523, Brest) and William Drennan (RSMAS, Miami) for providing the SHOWEX data, and Jeffrey Harris (ENPC/LHSV) for many fruitful discussions in the course of this study.

8. REFERENCES

Alves, J.-H., Banner, M. (2003). Performance of a Saturation-Based Dissipation-Rate Source Term in Modeling the Fetch-Limited Evolution of Wind Waves. *J. Phys. Oceanography*, 33, 1274-1298.

Ardhuin, F., Rogers, E., Babanin, A.V., Filipot, J.-F., Magne, R., Roland, A., van der Westhuysen, A.J., Queffeulou, P., Lefevre, J.-F., Aouf, L., Collard, F. (2010). Semiempirical dissipation source functions for ocean waves. Part I: Definition, calibration, and validation. *J. Phys. Oceanography*, 40, 1917-1941.

Ardhuin, F., Herbers, T.H.C, van Vledder, G., Watts, K., Jensen, R., Graber, H.C. (2007). Swell and Slanting-Fetch Effects on Wind-Wave Growth. *J. Phys. Oceanography*, 37, 908-931.

Ardhuin, F., Herbers, T., Jessen, P., O'Reilly, W. (2003a). Swell Transformation across the Continental Shelf. Part II: Validation of a Spectral Energy Balance Equation. *J. Phys. Oceanography*, 33, 1940-1953.

Ardhuin, F., Herbers, T., O'Reilly, W., Jessen, P.F. (2003b). Swell Transformation across the Continental Shelf. Part I: Attenuation and Directional Broadening. *J. Phys. Oceanography*, 33, 1921-1939.

Benoit, M., Marcos, F., Becq, F. (1996). Development of a Third Generation Shallow-Water Wave Model with Unstructured Spatial Meshing. *Proceedings of the 25th International Conference on Coastal Engineering (ICCE'1996)*, 465-478, Orlando (FL, USA).

Donelan, M. (1987). The effect of swell on the growth of wind waves. *Johns Hopkins APL Tech. Dig., 8*, 18-23.

Du, J., Bolaños, R., Guo Larsén X. (2017). The use of a wave boundary layer model in SWAN, *J. Geophys. Res. Oceans*, 122, 42-62.

Hasselmann, K. (1974). On the spectral dissipation of ocean waves due to white capping. *Bound.-Layer Meteor.*, 6, 107-127.

Hasselmann, S., Hasselmann, K., Allender, J., Barnett, T. (1985). Computation and parameterizations of the nonlinear energy transfer in a gravity-wave spectrum. Part II: Parameterizations of the nonlinear energy transfer for application in wave models. *J. Phys. Oceanography*, 15, 1378-1391.

Hwang, P.A., García-Nava, H, Ocampo-Torres, F.J. (2011). Observations of Wind Wave Development in Mixed Seas and Unsteady Wind Forcing. *J. Phys. Oceanography*, 41, 2343-2362.

Janssen, P.A.E.M, Bidlot, J.-R. (2021). On the consequences of nonlinearity and gravity-capillary waves on wind-wave interaction. ECMWF Tech. Memo., 42pp.

Janssen, P.A.E.M. (1991). Quasi-linear Theory of Wind-Wave Generation Applied to Wave Forecasting. *J. Phys. Oceanography*, 21, 1631-1642.

Komen, G.J., Hasselmann, S., Hasselmann, K. (1984). On the Existence of a Fully Developed Wind-Sea Spectrum. *J. Phys. Oceanography,* 14, 1271-1285.

Monin, A.S., Obukhov, A.M. (1954). Basic laws of turbulent mixing in the surface layer of the atmosphere. *Tr. Akad. Nauk SSSR Geophiz. Inst.,* 24, 163-187.

Shemer, L. (2019). On Evolution of Young Wind Waves in Time and Space. *Atmosphere,* 10, 562, 54pp.

van de Westhuysen, A.J. (2007). Advances in the spectral modelling of wind waves in the nearshore. *Ph.D. thesis, Delft University of Technology, Delft, The Netherlands.* 206 pp.

Villefer, A., Benoit, M., Violeau, D., Luneau C., Branger, H. (2021). Influence of Following, Regular, and Irregular Long Waves on Wind-Wave Growth with Fetch: An Experimental Study. *J. Phys. Oceanography,* 51, 3435-3448.

Zhang, F., Drennan, W., Haus, B., Graber, H. (2009). On wind-wave-current interactions during the Shoaling Waves Experiment. *J. Geophys. Res. Oceans,* 114, C01018.